Pathways and watermass transformation of Atlantic Water entering the Nordic Seas through Denmark Strait in two high resolution ocean models

Ypma, S. L.; Brüggemann, N.; Georgiou, S.; Spence, P.; Dijkstra, H. A.; Pietrzak, J. D.; Katsman, C. A.

DOI
10.1016/j.dsr.2019.02.002

Publication date
2019

Document Version
Accepted author manuscript

Published in
Deep-Sea Research Part I: Oceanographic Research Papers

Pathways and watermass transformation of Atlantic Water entering the Nordic Seas through Denmark Strait in two high resolution ocean models

S.L. Ypma[a,*], N. Brüggemann[b], S. Georgiou[a], P. Spence[c], H.A. Dijkstra[d], J.D. Pietrzak[a], C.A. Katsman[a]

[a] *Department of Hydraulic Engineering, Delft University of Technology, Civil Engineering and Geosciences, Environmental Fluid Mechanics, Delft, Netherlands.*
[b] *Faculty of Mathematics, Informatics and Natural Sciences, University of Hamburg, Hamburg, Germany.*
[c] *Climate Change Research Centre, University of New South Wales, Sydney, New South Wales, Australia.*
[d] *Institude for Marine and Atmospheric Research Utrecht, Utrecht University, Netherlands.*

Abstract

The pathways and watermass transformation of the North Icelandic Irminger Current (NIIC) in the Nordic Seas are investigated by tracing the NIIC watermass in two ocean circulation models: the Modular Ocean Model (MOM) and the Parallel Ocean Program (POP). The two simulations use identical atmospheric forcing and have a horizontal resolution of 0.1°. However, the models differ strongly in their representation of the sea-ice cover in the Nordic Seas and, possibly as a consequence, display a different hydrography. Results from observational studies point towards a fast overturning loop north of Iceland that connects the NIIC watermass to the Denmark Strait Overflow Water (DSOW). However, our Lagrangian analysis shows that only 0.2

*Corresponding author: Stefanie Ypma , s.l.ypma@tudelft.nl, Environmental Fluid Mechanics, Stevinweg 1, 2628 CN, Delft, The Netherlands

Sv of the entering NIIC water exits as DSOW in the two models. In POP, the main transformation to dense water takes place along a short path north of Iceland. In MOM however, the contributing part of the NIIC to DSOW takes a long path through the Nordic Seas and reaches Denmark Strait as part of the East Greenland Current (EGC). A small contribution of the NIIC watermass to the Iceland Scotland Overflow Water (ISOW) is found in both MOM and POP (7.8%, respectively 2.1% of the NIIC watermass). In the model simulations studied, the part of the NIIC watermass that is not connected to the overflows takes many different pathways through the Nordic seas. Analysis of the depth distribution and the thermohaline changes of the particles indicates that the watermass transformation that takes place north of Iceland is crucial for diversifying the pathways of the NIIC water.

Keywords: North Icelandic Irminger Current, North Icelandic Jet, Denmark Strait Overflow Water, Water mass transformation, Nordic Seas, Atlantic Water pathways

1. Introduction

The transformation of Atlantic Water (AW) north of the Greenland-Scotland Ridge is one of the key mechanisms for controlling the strength of the Atlantic Meridional Overturning Circulation (AMOC) via the overflows through Denmark Strait and across the Iceland-Scotland Ridge. The warm AW flows poleward into the Nordic Seas and beyond through three main gateways (see schematic in Figure 1) (e.g. Hansen and Østerhus, 2000). Two of these, through which the majority of the AW flows north, are located east of Iceland. West of Iceland, AW is transported by the North Icelandic Irminger

Current (NIIC). This third branch flows north along the western Icelandic slope and has been monitored since 1985 (e.g. Jónsson and Valdimarsson, 2005), though the fate of the NIIC has only recently been studied in more detail. Water mass transformation of the AW in the NIIC is thought to be linked to the densest part of the Denmark Strait Overflow Water (DSOW) (Våge et al., 2011). However, as of yet it is unclear which path the NIIC takes after entering the Nordic Seas and where watermass transformation from the NIIC to DSOW takes place. The aim of this study is to investigate the paths and watermass transformation of the NIIC in detail in two ocean models using a Lagrangian approach.

Previous studies suggest three possible pathways for the NIIC. The first path was described by Swift and Aagaard (1981) as well as Jónsson (1992), who observed Atlantic Water at the north Icelandic continental shelf, without any propagation into the central Iceland Sea. They found that east of Iceland the water leaves the shelf and propagates in the direction of the Norwegian Sea. Stefánnson (1962) showed that part of the NIIC watermass mixes with surface water from the Iceland Sea, forming a watermass that connects to the Iceland Scotland Overflow Water (ISOW).

ISOW, which has a similar magnitude as DSOW, is formed by a mixture of watermasses that, combined, are generally labelled as Modified East Icelandic Water (MEIW). The main constituents of the MEIW are the North Icelandic Winter Water, the East Icelandic Water, the Norwegian Sea Deep Water and the Norwegian North Atlantic Water, where the latter is partly formed by transformation of the NIIC watermass (e.g. Hansen and Østerhus, 2000). The main outlet of these watermasses is through the Faroe-Shetland Channel.

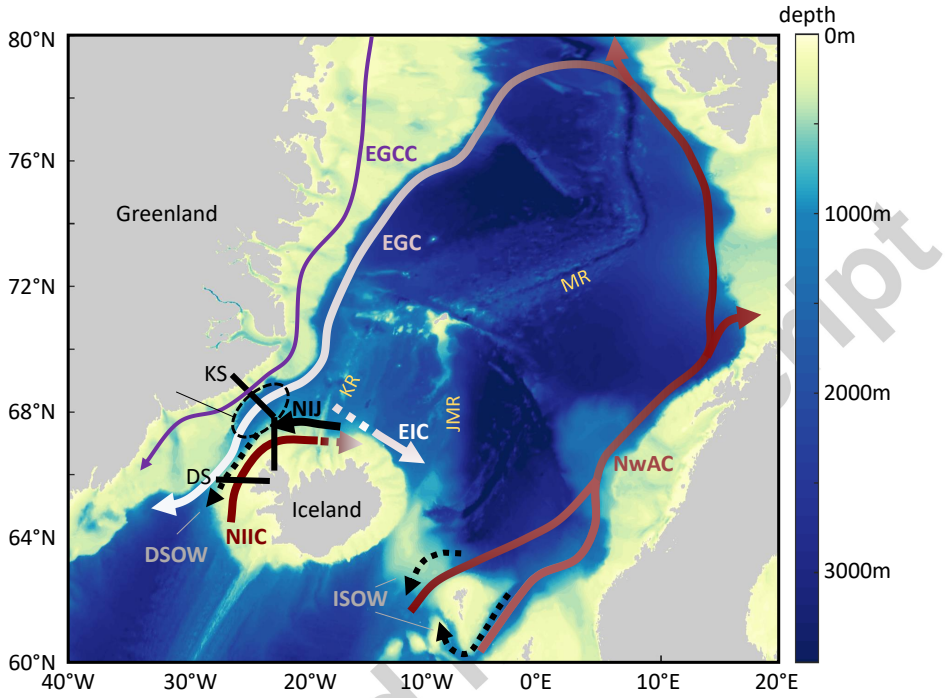

Fig. 1: Schematic of the circulation in the Nordic Seas and bathymetry. Shown in red are the warm and salty inflowing currents: the North Icelandic Irminger Current (NIIC) and the Norwegian Atlantic Current (NwAC). The East Greenland Current (EGC) and the East Icelandic Current (EIC) are shown in white and the East Greenland Coastal Current (EGCC) in purple. Dense currents are shown in black: the North Iceland Jet (NIJ), the Denmark Strait Overflow Waters (DSOW, dashed line) and the Iceland Scotland Overflow Waters (ISOW, dashed lines). The bathymetric features pertinent for this study are indicated in yellow: the Kolbeinsey Ridge (KR), the Jan Mayen Ridge (JMR) and the Mohn Ridge (MR). The release location of the particles at 66°N in Denmark Strait (DS) and the Kögur Section (KS) are shown in black. Note that the bathymetry is from ETOPO2v2, and not the model bathymetry.

Using surface drifters, Valdimarsson and Malmberg (1999) observed a second possible path for the NIIC, where most of their drifters seemed to be topographically steered northward by the Kolbeinsey Ridge (see Figure 1) and returned south through Denmark Strait in the East Greenland Current (EGC).

More recently, analyses from multiple hydrographic transects along the coast of Iceland suggested a third possible pathway. They point to a close relationship between the NIIC and the North Icelandic Jet (NIJ) (e.g. Våge et al., 2011, 2013, 2015). The NIJ transports the densest component of the Overflow Water through Denmark Strait (Våge et al., 2011). The other two currents advecting dense water from the north through the strait are the shelf break current and the separated branch of the EGC (Harden et al., 2016). The observations show several indications of a connection between the NIIC and the NIJ. First, both currents can be traced along the continental slope of Iceland until their signal disappears at the northeast corner of the island (Våge et al., 2011). Along the Icelandic shelf, the currents seem to be dynamically linked by sharing a pronounced density front (Pickart et al., 2017). Second, the volume transport of both currents is very similar. It is estimated to be 1 Sv and 0.88 Sv for the NIJ and NIIC, respectively (Jónsson and Valdimarsson, 2012; Harden et al., 2016).

Våge et al. (2011) showed, by using an idealized model set-up, that the mechanism that links the NIIC and the NIJ is similar to the one described by e.g. Spall (2004) and Straneo (2006). These studies suggest that buoyant water from the NIIC is transported to the interior of the Iceland Sea by eddies due to baroclinic instability of the NIIC. In these idealized models, the heat

flux from the boundary current to the interior balances the atmospheric cooling over the interior that induces convection. The dense watermass returns to the Icelandic slope where it sinks and forms the NIJ.

So far, follow-up studies have not been able to corroborate the connection between the NIIC and the interior of the Iceland Sea. Using measurements from eight shipboard surveys, Pickart et al. (2017) find a strong, in phase correlation in salinity between the NIJ and NIIC. In case the two currents are linked, this would imply the existence of a very fast overturning. To accomodate this short time-scale, they hypothesize that the overturning can not take place in the central Iceland gyre, but instead takes place northwest of the gyre where deep mixed layers are observed. In their discussion it remains unclear how the water of the NIIC reaches this area. Additionally, de Jong et al. (2018) do not find a connection between the interior Iceland Sea and the NIJ either. In their study, based on the analysis of deployed RAFOS floats, they highlight the importance of the East Icelandic Current (EIC, Figure 1) that potentially blocks the exchange between the Iceland Sea gyre and the Icelandic slope region. This branch might not be captured by the idealized model of Våge et al. (2011). Tracking the NIJ watermass back in time in a high resolution ocean model (Viking20) leads to a similar insight: no exchange with the interior of the Iceland Sea is seen and most of the NIJ originates from the shelfbreak EGC (Behrens et al., 2017). It is therefore still unclear what role the NIIC plays for the formation of Denmark Strait Overflow Waters.

Lagrangian studies as Behrens et al. (2017) can be very useful as particle tracking in global ocean models has the advantage that a large number of

particles can be used in comparison to observations, providing better statistics of variable pathways. However, different ocean models lead to different conclusions. For example, backtracking the overflow waters in the 1/20° horizontal resolution Viking20 ocean model, Behrens et al. (2017) find that the bulk part of the Denmark Strait Overflow Water in the model (60%) has an Arctic origin. In contrast, in the 1/10° ocean model used by Köhl (2010) the largest part of the DSOW originates from watermass transformation taking place within the Nordic Seas. Köhl (2010) argues that the pathways vary spatially depending on the magnitude of the wind stress. Thus, he concluded that the differences in ocean models regarding forcing and set-up may lead to significantly different results.

In addition to the variables mentioned by Köhl (2010), the horizontal resolution, discretization in the vertical, topography, mixing parameterizations and boundary conditions like applied atmospheric forcing and sea-ice conditions impact the mixed layer dynamics and therefore the circulation in the models (Willebrand et al., 2001; Langehaug et al., 2012; Courtois et al., 2017). A correct representation of the convection regions is crucial for the transformation processes of watermasses. However, ocean models still show large differences in mixed layer depth, both in low- and high resolution ocean models (e.g. Tréguier et al., 2005; Danabasoglu et al., 2014).

The aim of this study is to investigate to what extent the inflowing Atlantic Water through Denmark Strait contributes to the Overflow Water and whether its transformation is related to the location of convection regions within the Nordic Seas as proposed by Våge et al. (2011). A Lagrangian perspective is chosen, where the NIIC watermass entering the Nordic Seas

through Denmark Strait is tracked in two ocean models that differ substantially in their representation of deep convection: the Modular Ocean Model (MOM) and the Parallel Ocean Program (POP). The models have the same horizontal grid with a resolution of 0.1° degree and identical atmospheric forcing. However, their sea-ice representation and consequently the hydrography in the Nordic Seas is different. This paper presents the pathways of the NIIC water in these two models, a quantification of the contribution of the NIIC to the overflows and a discussion on where and how the NIIC watermass is transformed.

The paper is structured as follows. Section 2 describes the model simulations analysed and the particle tracking method. In section 3 the performance of both models in the Nordic Seas is compared to observations. This is followed by the main results of this study, where the pathways of the NIIC watermass are described in detail in section 4 and the watermass transformation along the pathways is discussed in section 5. A discussion and the conclusions are provided in section 6.

2. Methods

In this study, a Lagrangian analysis is conducted to trace the NIIC watermass. Numerical particles are advected offline using the velocity fields of the model output. The particles' location, depth, temperature and salinity are saved and used to determine the pathways and watermass transformation of the NIIC water. This method is applied to two ocean models that differ substantially in their representation of deep convection and sea ice in order to investigate the sensitivity of the results to the location of deep mixed

layers and heat fluxes.

2.1. Global ocean model configurations

The particles are advected in the Modular Ocean Model global ocean-sea ice model (MOM) and the Parallel Ocean Program ocean-only model (POP). The ocean model configurations are described in detail by Spence et al. (2017) (MOM) and Weijer et al. (2012) (POP) and form the ocean component of frequently-used climate models (MOM in GFDL-CM2.6 and POP in CESM1.0). The models have the same horizontal resolution of 0.1° and use a tripolar B-grid. This yields ∼4.5 km resolution at 65°N. Nurser and Bacon (2014) estimated the first Rossby Radius of deformation to be ∼7 km in the Norwegian Sea and ∼3 km in the Iceland and Greenland Sea. Therefore, these ocean models are only partly eddy resolving in the region of interest. In the vertical, MOM (POP) has 50 (42) layers with a resolution of 5m at the surface up to 200m (250m) in the deeper layers.

Both models are forced by prescribed atmospheric conditions using the Coordinated Ocean-ice Reference Experiments Normal Year Forcing (COREv2-NYF) reanalysis data (Griffies et al., 2009; Large and Yeager, 2009). COREv2-NYF provides a climatological mean atmospheric state estimate at 6-hour intervals at roughly 2° horizontal resolution. The atmospheric state is converted to ocean surface fluxes by bulk formulae, so there are no air-sea feedbacks. The Normal Year Forcing is derived from 43 years of the interannual varying atmospheric state from 1958 to 2000. Since the same seasonal forcing is applied every year, the interannual variability is small. Using normal year forcing is advantageous for this study as the results will not depend on the release year of the numerical particles. For practical reasons, only one year

of velocity data representative for the mean ocean state of the models is used in this study.

The KPP parameterization is used for the parameterization of convection in both models (Large et al., 1994). Further, vertical viscosities and diffusivities are set by KPP and in the horizontal, biharmonic viscosity and diffusion are used. In MOM, the surface salinity is restored on a 60-day timescale. In POP, the surface salinity is restored during the first 75 years of the spin-up period. From that moment onwards, 'mixed boundary conditions' are applied, derived from the monthly-averaged restoring flux of the final five years of the spin-up.

The models differ in their sea-ice configurations. MOM is coupled to the GFDL Sea Ice Simulator model, so the sea ice evolves freely. In POP, the sea-ice edge is fixed and defined by the -1.8°C isotherm of the SST climatology from COREv2-NYF. Under the diagnosed sea ice, temperature and salinity are restored with a timescale of 30 days. The approaches regarding the sea-ice configurations in MOM and POP lead to large differences in the maximum sea-ice extent in the Nordic Seas, as shown by the black line in Figures 2b and 2c. In POP the maximum sea-ice extent is confined to the continental shelves of Greenland, whereas in MOM the sea ice covers most of the Greenland and Iceland Seas in winter months. Additionally, Figure 2 shows that the modeled hydrographic fields of the two models differ as well. Section 3 will further elaborate on these differences with respect to observations.

2.2. Tracking the Atlantic Water north through Denmark Strait

Lagrangian particles are released daily for a duration of one year in the northward flowing Atlantic Water in Denmark Strait. The particles are re-

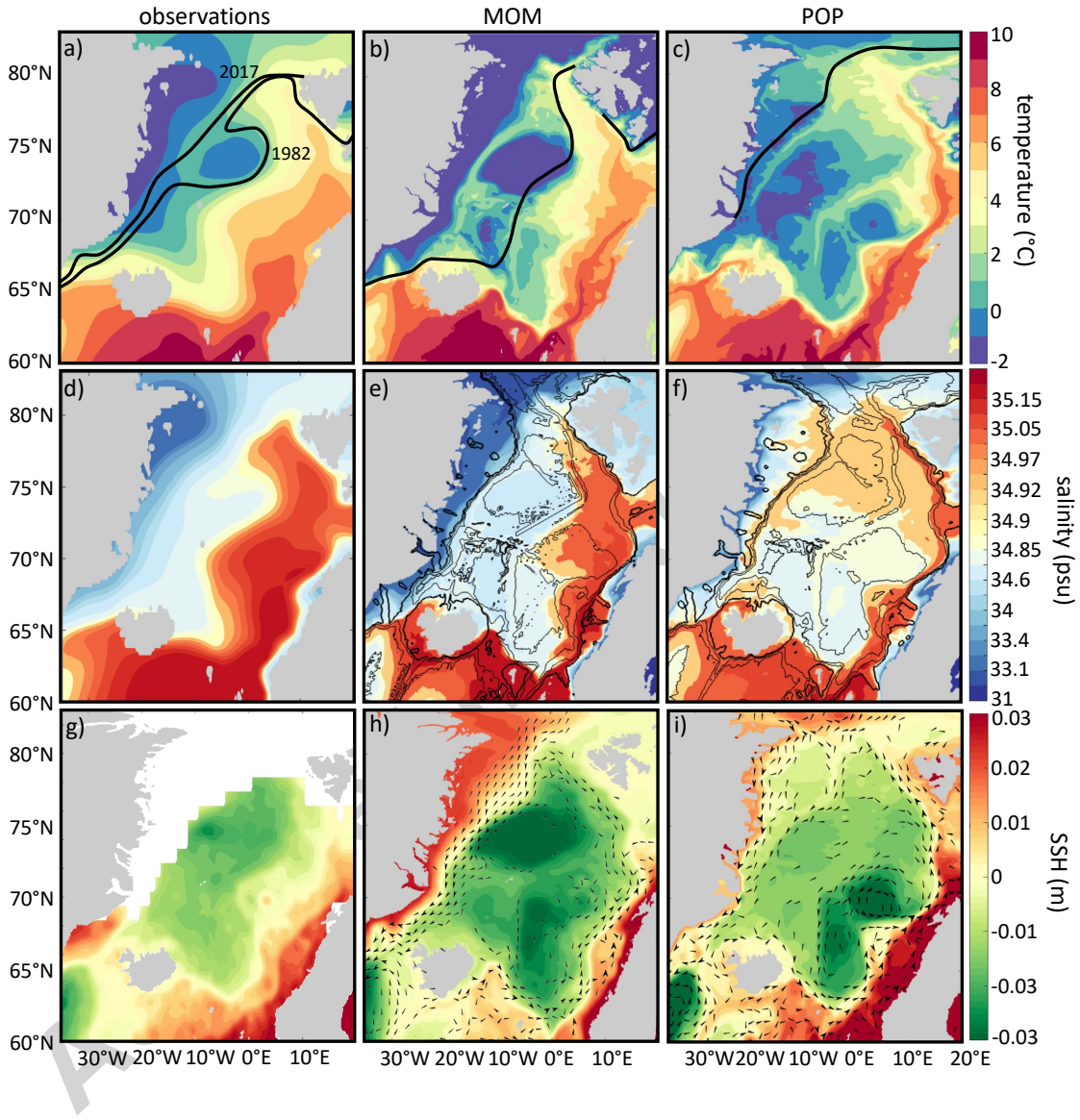

Fig. 2: Mean temperature (top) and salinity (middle) at 50m depth and sea surface height (bottom) from (a,d,g) observations, (b,e,h) MOM and (c,f,i) POP. The observational hydrographic fields show the mean from 1995 to 2010 and are obtained from the Climatological Atlas of the Nordic Seas (Korablev et al., 2014). Panel (g) shows the mean absolute dynamic topography over the same period from the AVISO satellite altimetry. The black lines in (a-c) indicate the sea-ice extent in March. In (a) the extent in 1982 and 2017 are shown from the Sea Ice Index (Fetterer et al., 2017). The contour lines in (e) and (f) show the model isobaths at 400m (thick black line), 1000m, 1500m and 3000m depth. The black arrows in (h) and (i) show the mean surface velocity field for flow stronger than 0.05 m/s.

leased at a zonal transect at 66°N between Iceland and 28.9°W (black line in Figure 1 in Denmark Strait) at a resolution of 0.1° longitude and 20m in the vertical. The particle is only traced when the initial meridional velocity is positive (hence flowing to the north) and when the initial temperature is higher than 5°C (hence Atlantic Water). Each particle is tagged with its corresponding volume transport that is defined as the meridional velocity multiplied by the area of the cell face in which the particle is released (Döös, 1995).

The particles are advected forward in time with a timestep of 1 hour within the daily averages of the 3D velocity field output of the ocean model using the Connectivity Modeling System (CMS) (Paris et al., 2013). The CMS model uses a tricubic interpolation spatially, and a 4^{th} order Runge Kutta stepping scheme in time. No horizontal or vertical diffusivity is added to the particles, so the particle motion is purely advective. Mixing is only taken into account as far as it is represented by resolved eddies. The CMS model does include the option to parameterize the vertical movement in mixed layers by adding a random kick in the vertical to the particle trajectories (van Sebille et al., 2013). Results of including this option are compared to results without the parameterization, and no significant changes were found in the particle pathways and the watermass transformation along the paths. The change in density of the particles in the convection region defines the future path, as the particles have to follow isopycnals. It does not matter at which depth the particle is located within the mixed layer, since the T-S properties of the mixed layer are continuously homogenized by the convective adjustment used in the model simulations. Therefore, the results of the

CMS model without the parameterization of the vertical movement in mixed layers have been used in this study.

In total 226407 (284412) particles are tracked in MOM (POP). The total advection time of the particles is chosen to be 6 years and is executed by looping through the available dataset of one year of model output. The resulting pathways and timeseries of temperature and salinity of the particles do not show large variations from the end of December to the beginning of January, which justifies this method. After six years, the majority of the particles has left the Nordic Seas (81% in MOM and 69.8% in POP, see section 4 and Figure 6).

The resulting pathways are then visualized using a particle density plot (see section 4 and Figure 5). To this end every particle location is regridded on a 0.1°x 0.1° latitude-longitude grid. Each position can only be occupied by the same particle once, to avoid the obscuration of the pathways by long residence times as described by Behrens et al. (2017). The particle density is given by the transport carried by the particles at each location divided by the total transport. This way, the paths that the particles are most likely to take are highlighted.

3. Model performance in the Nordic Seas

Apart from the different sea-ice configuration and the SSS restoring, the set-up of the two models is very similar, as described in section 2.1. Still, the resulting hydrography and circulation is remarkably different. In this section, a comparison of the two models is made and the modeled fields are validated against observations to highlight possible consequences of the different model

configurations. Also, the interpretation of the findings from the Lagrangian approach in sections 4 and 5 requires knowledge of the Eulerian background velocity and hydrography. The first part of this section compares the Nordic Seas hydrography and the mixed layer depth from each model to observations. The second part addresses the circulation in both models and the third part discusses the hydrography at the Kögur section (see Figure 1) to investigate the properties of the NIIC and the Denmark Strait Overflow Water.

3.1. Hydrographic properties

The mean temperature and salinity at 50m depth of both models is compared to the observed fields of the Nordic Seas from 1995 to 2010 in Figure 2a-f. A depth of 50m is chosen, since at this depth the difference in temperature between the eastern and western basins is more pronounced than at the surface. Apart from some local discrepancies, both models compare well to the observed hydrography in the Nordic Seas. The hydrographic fields in MOM differ from the observations on the western side of the Nordic Seas. The Greenland Sea and Iceland Sea are colder than observed (ΔT$\sim$2°C, Figure 2b) and the waters near the Greenland coast are too fresh (ΔS$\sim$0.5 psu, Figure 2e). In POP, a warm and saline signal that is not present in observations, seems to propagate onto the northern Greenland shelf region at 80°N (Figures 2c and 2f). Furthermore, the lateral spread of the Atlantic Water throughout the eastern basins is minimal in POP. Instead, a local minimum in temperature is seen in both the Lofoten Basin and the Norwegian Basin (Figure 2c). Further, the Atlantic Water returning in the EGC is warmer in MOM than in POP, indicating that the boundary current in POP loses more heat than the boundary current in MOM (see also table 1).

The location where deep convection takes place in both models is very different. Figure 3a and 3b show the maximum mixed layer depth (MLD) in MOM and POP. In order to use a common criterion for both models, the MLD is defined as the depth where the density difference compared to the surface is larger than 0.125 kg/m^3 as described in Danabasoglu et al. (2014). The density is determined from the temperature and salinity fields using the UNESCO nonlinear equation of state (Millero and Poisson, 1981). The maximum in MLD is reached at the end of winter and beginning of spring. The models display a clear difference in both the magnitude and the location of deep convection. In MOM the convection reaches 1000m depth, and the deepest mixed layers are seen southwest of Svalbard and within the Norwegian Atlantic Current (Figure 3a). In contrast to MOM, POP has mixed layers with a maximum of 1500m depth along the shelf break of Greenland, into the Greenland Basin and north of the Icelandic Plateau (Figure 3b).

The location and depth of deep convection are strongly dependent on the atmospheric forcing, the sea ice and the stratification of the water column (e.g. Moore et al., 2015; Harden et al., 2015; Våge et al., 2018). Comparing the location and the depth of the deep convection to the atmospheric heat flux (contours in Figure 3) and the sea-ice edge in March (dashed lines in Figure 3) confirms this. In MOM the edge of the deep convection region coincides with the -100 W/m^2 heat flux contour (Figure 3a). Furthermore, it is clear that the deep convection in the western basin is absent because the sea ice is preventing the cooling of the ocean surface by the atmosphere. In POP the sea-ice edge, which is located much closer to the Greenland coast

(see dashed line in Figure 3b), also plays an important role for the location of the deep convection. The strongest heat fluxes are found along the sea-ice edge, which makes the water column more prone to deep convection.

Observational estimates of the mixed layer depth in the Nordic Seas are limited due to the lack of year-round observational data. Mixed layers with depths of 560m have been observed in the Lofoten and Norwegian Basins (Nilsen and Falck, 2006; Richards and Straneo, 2015). The deep convection in the Greenland Sea is highly variable and can extend to depths of 2000m (Rudels et al., 1989; Latarius and Quadfasel, 2016). Combining all available observational data in the Iceland Sea, Våge et al. (2015) found that the deepest mixed layers in this basin (∼300m) are located in the northwest, close to Greenland. These findings suggest that the deep convection in the Greenland Sea is better represented in POP and the deep convection in the Lofoten Basin is better represented in MOM. Further, POP overestimates the maximum MLD in the Iceland Sea, whereas in MOM deep convection does not occur in this region. These differences are likely a direct consequence of the difference in sea-ice behavior between the models. Recall that the sea-ice extent in POP is fixed to observed values, whereas in MOM the sea ice is dynamically active. Apparently, the sea-ice model used in MOM is overestimating the sea-ice extent in the Nordic Seas, which suppresses deep convection in the western basins.

3.2. Nordic Seas Circulation

The circulation pattern in the Nordic Seas is strongly controlled by topography, while the strength of the circulation is influenced by the wind

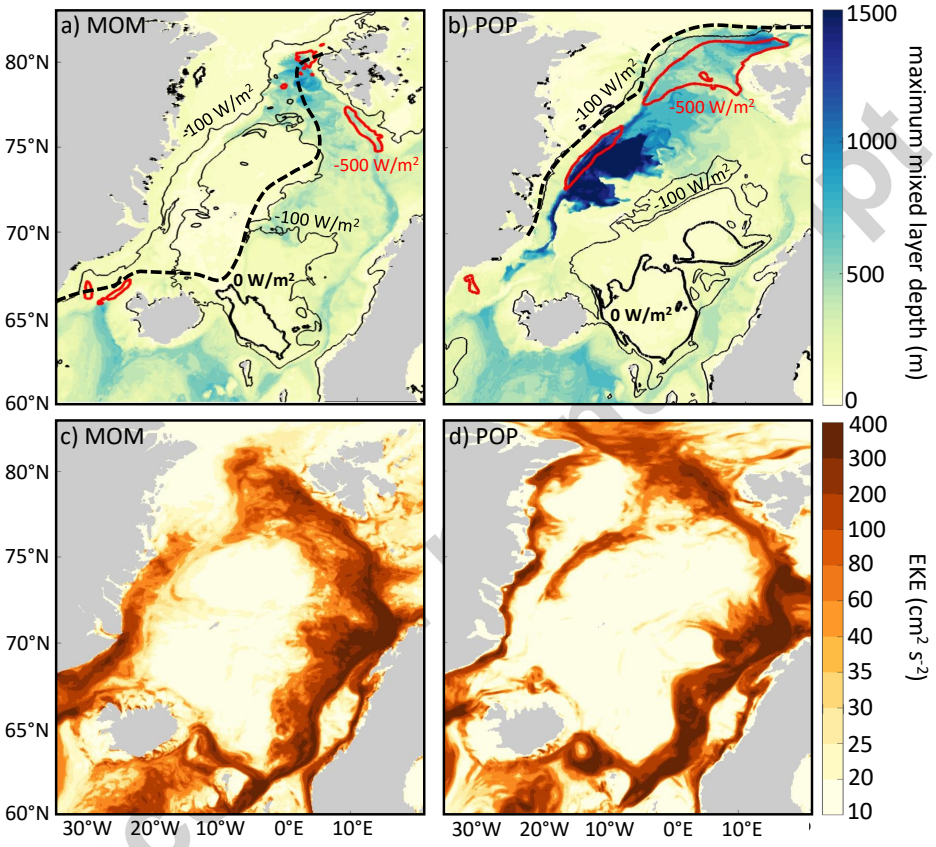

Fig. 3: Maximum mixed layer depth (top) and eddy kinetic energy (bottom) for MOM (left) and POP (right). Solid contours in (a) and (b) show the -500 W/m^2 (in red), -100 W/m^2 and 0 W/m^2 (in black) March mean heat flux. The dashed contours indicate the sea-ice extent in March.

forcing and hydrography (e.g. Blindheim and Østerhus, 2005; Spall, 2010). Figures 2g-i show the mean sea surface height (SSH) from observations, and in MOM and POP. The SSH in both models compares quite well to observations, except in the Lofoten Basin. Especially in POP a depression in SSH is clearly seen in the Lofoten Basin, whereas a positive SSH anomaly is commonly observed in this area associated with the Lofoten Vortex (e.g. Søiland et al., 2016; Fer et al., 2018). The arrows in Figures 2h and 2i show the mean surface velocity in both models. The location and direction of the currents compare well to the observed surface circulation derived from drifters by e.g. Jakobsen et al. (2003). The model results differ regarding the strength of the currents. POP has a very strong cyclonic gyre in the Lofoten Basin and the Norwegian Basin, but the circulation in the Greenland and Iceland Basin is weaker. In MOM cyclonic gyres are most pronounced in the Greenland Basin and the Norwegian Basin. As the EGC in POP is very weak (see also table 1), most Arctic Water is transported southwards by the East Greenland Coastal Current. In MOM this current is less pronounced.

When the circulation is compared to the structure of deep convection in the basin (Figures 2h-i to 3a-b), the regions with convective activity coincide with regions of low velocity in both models. This seems contradictory at first, since deep convection in the interior of ocean basins is thought to be positively correlated with the strength of the cyclonic boundary current that is surrounding the basin: as the interior of the ocean basin is cooled during winter, the temperature gradient between the boundary current and the interior increases and the boundary current strengthens as a result of the thermal wind balance (e.g. Spall, 2004; Tréguier et al., 2005). However, in

our simulations a strong cooling coincides with a weak temperature gradient between the interior and the boundary current and therefore with a reduced geostrophic transport. The reduced temperature gradient is probably caused by the stronger cooling over the boundary current area compared to the interior. This heat loss seems to be so strong that the supply of warm water from the boundary current upstream is not sufficient and thereby, the boundary current temperature decreases.

The eddy kinetic energy (EKE) is shown is Figures 3c-d. Although the model resolution is not sufficient to fully resolve all eddy activity in the Nordic Seas, most of the variability is captured. The largest eddy variability is seen west of the Lofoten islands. Here, the EKE exceeds 400 cm^2s^{-2}, which compares relatively well to observational estimates (e.g. Wekerle et al., 2017). North of Iceland a small band of increased EKE from the NIIC can be seen. Both observational estimates of the eddy variability in this region and estimates from higher resolution model simulations show slightly larger values for EKE of $\sim$100 cm^2s^{-2} compared to $\sim$60 cm^2s^{-2} in MOM and POP (e.g Jakobsen et al., 2003; Wekerle et al., 2017).

3.3. Hydrographic properties at Kögur section

Next, the properties of the inflowing Atlantic Water and the outflowing Overflow Water through Denmark Strait are compared between the models and mooring observations at the Kögur section (Harden et al., 2016). This transect is well documented from observations and the characteristics of both the inflowing NIIC and the outflowing dense waters can be distinguished along the section. Further, to enable direct comparison between the models and observations, table 1 shows the mean temperature, salinity and volume

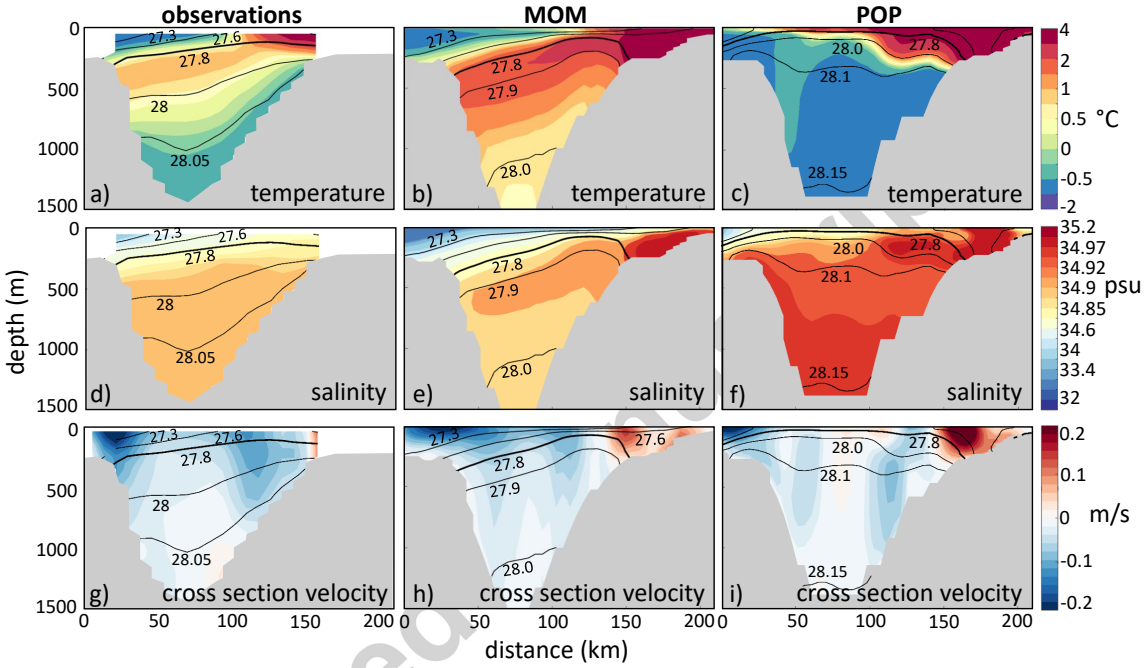

Fig. 4: Sections of temperature (top), salinity (middle) and cross section velocity (bottom) at the Kögur section (transect given in Figure 1). The x-axis shows the distance along the transect, starting at the Greenland coast. Positive velocity indicates northward flow. The left column shows the mean fields from observations described by Harden et al. (2016). The middle and right column show the mean fields of MOM and POP respectively. Density is given by the contourlines, where the thick black line corresponds to $\sigma = 27.8$ kg/m^3. Note that the colorbars for temperature and salinity are non-linear.

	NIIC			DSOW			NIJ			EGC (76°N)		
	obs	MOM	POP	obs	MOM	POP	obs	MOM	POP	obs	MOM	POP
Ψ (Sv)	1.1[1]	1.1	1.8	3.2[4]	2.5	3.1	1±0.17[6]	0.5	1.3	5-7[7]	7.5	2.8
T (°C)	3-6[2]	6.2	6.6	0.1-0.5[5]	2.5	-0.5	-0.4-0[3]	1.4	-0.4	2-4[7]	2.3	0.7
S (psu)	35-35.15[3]	35	35.1	34.82-34.94[5]	34.9	35	34.9-34.91[3]	34.9	35	34.9-35.1[7]	34.9	35

Table 1: Mean transport (Ψ), temperature (T) and salinity (S) of the NIIC, DSOW, NIJ and EGC from observations and the model simulations. Observational values are estimated from [1] Våge et al. (2013), [2] Jónsson and Valdimarsson (2005), [3] Pickart et al. (2017), [4] Jochumsen et al. (2017), [5] Eldevik et al. (2009), [6] Harden et al. (2016) and [7] Håvik et al. (2017).

transport estimates of the NIIC, DSOW, NIJ and EGC.

Figure 4 shows the mean temperature, salinity and the cross-section velocity (positive indicates northward flow) at the Kögur section. The mean temperature along the Kögur transect in MOM captures the observed pattern well (Figure 4b), although the deep waters are too warm (ΔT$\sim$1°C, Figure 4b). In POP, the stratification is much stronger than observed, with warmer water at the surface (ΔT$\sim$ +2°C) and colder waters below (ΔT$\sim$-1.5°C, Figure 4c). The salinity shows similar discrepancies, where the surface and deep layers are too fresh in MOM and too salty in POP by $\sim$0.1 psu compared to the observations (Figures 4e and 4f). Combining the findings for temperature and salinity, the in- and outflowing waters in MOM are slightly too light and the in- and outflowing waters in POP are too dense.

In the cross-section velocity at the Kögur section different branches can

be distinguished (Figures 4g-i). The NIIC is present in both models and is characterized by a warm and salty water mass flowing north on the Icelandic shelf. The NIIC transport is 1.1 Sv in MOM and 1.8 Sv in POP compared to 0.88-1.1 Sv estimated from observations (Jónsson and Valdimarsson, 2012; Våge et al., 2013). As a result of the model bias in density, the overflow water is characterized by different isopycnals. The 27.8 kg/m^3 respectively 28.0 kg/m^3 isopycnals are chosen to represent the overflow water mass in MOM and POP. This results in an overflow transport into the Atlantic of 2.4 Sv in MOM and 3.1 Sv in POP, which is slightly lower than the observed estimate of 3.2 Sv from Jochumsen et al. (2017). Compared to observations, the NIJ is better represented in POP than in MOM (see table 1).

In summary, this section discussed the differences between the models and observations. Overall, the models capture the main characteristics of the Nordic Seas well, but disagree on the location of deep mixed layers, the gyre strength in the Nordic Seas and the hydrographic characteristics of the Denmark Strait Overflow Water. The remainder of this paper will focus on whether these differences influence the pathways of the NIIC water and the location and strength of the watermass transformation.

4. Pathways of the NIIC watermass in the Nordic Seas

The density plot of the particles seeded in the NIIC (see section 2.2) reveals the pathways of the NIIC watermass in the Nordic Seas (Figure 5). After entering the Nordic Seas, most particles follow the 400m isobath around Iceland to the east (see inlays Figure 5). From there, multiple pathways can be identified following the shelfbreak and the main topographic features of

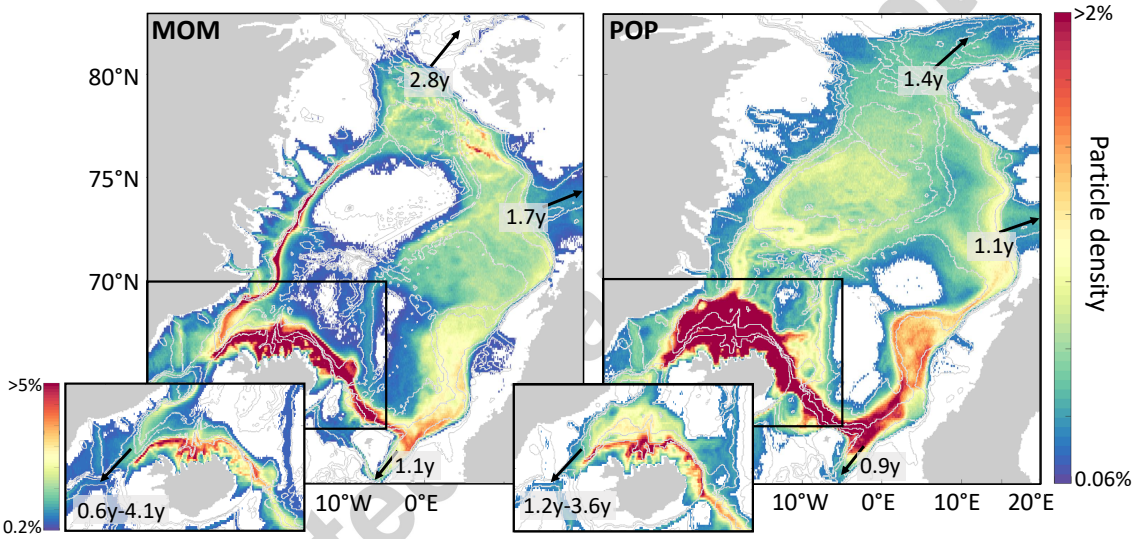

Fig. 5: Density plot of the particle position in MOM (left panel) and POP (right panel). The inlay shows the pathways near Iceland in more detail (note the different colorscale in the bottom left). The median travel time for the particles to reach the exits of the Nordic Seas is given in years.

the Nordic Seas; the Vring Plateau and the Jan Mayen- and Mohn Ridges (see Figure 1).

These particle density plots show that the paths along which the particles enter the interior of the Nordic Seas are completely different between the two models. Particles mainly occupy the Lofoten Basin in MOM, whereas in POP the particles occupy the Greenland Basin. In MOM, particles are captured by eddies near the Lofoten Islands and travel westward until they reach the Mohn Ridge. There, the majority of the particles flows to the north and eventually joins the EGC. In POP, the particles are not captured by eddies near the Lofoten islands, but are transported in the strong cyclonic gyre of the Lofoten Basin and the Norwegian Basin instead. At the western side of the Nordic Seas, particles travel throughout the Greenland Basin, without displaying one distinctive path.

The residence time of the particles within the Nordic Seas is highly variable and depends on where the particles leave the basin. The median travel time is given in Figure 5 for the particles that enter and leave the Nordic Seas within the time interval of 6 years (section 2.2). The shortest residence times of $\sim$1 year are found for particles taking a short path crossing the Greenland-Scotland Ridge, whereas the particles that follow the path along the rim of the Nordic Seas take $\sim$ 4 years to do so. On average, the travel time towards Fram Strait is one year shorter in POP than in MOM, which indicates that the particles flow much faster from the Lofoten Islands to Fram Strait in POP than in MOM.

In order to distinguish between the different paths, particles are selected based on which exit they take out of the Nordic Seas. This particle catego-

rization process is illustrated in Figure 6a. Furthermore, a selection is made based on whether particles enter the interior of the Nordic Seas, or stay close to the boundary with respect to the coastlines of Iceland, Norway, Svalbard and Greenland. Although the categorization is sensitive to the choice of the transects shown in Figure 6a, inspection of the individual particle trajectories indicates that the transect locations used in this study lead to a meaningful separation.

The result of this categorization process is summarized by Figures 6b and 6c. In both models, most of the NIIC watermass leaves the Nordic Seas toward the Atlantic Ocean by crossing the Greenland-Scotland Ridge (66.7% in MOM and 42.5% in POP). A smaller fraction of the NIIC watermass flows into the Arctic via Fram Strait or the Barents Sea (14.3% in MOM and 27.3% in POP). The part of the NIIC water that takes longer than 6 years to leave the Nordic Seas (19% in MOM and 30.2% in POP) is found mostly in the interior of the basin (not shown). A much longer advection time would be needed to advect all of the originally seeded NIIC particles out of the Nordic Seas.

The particles leaving the Nordic Seas through Denmark Strait can do so following different paths as indicated in Figures 6b-c; via a short loop north of Iceland (the DSs, short, path), via the rim of the Nordic Seas (the DSl, long, path), via the interior of the Nordic Seas (the DSm, middle, path) and via the coastal shelf area of Greenland (the DSc, coastal, path). As the connection of the NIIC to the overflow is the main interest of this study, the remainder of this paper is focused on the NIIC water returning to the Atlantic Ocean. Although the sea-ice cover, the mixed layers, and the transport of the NIIC

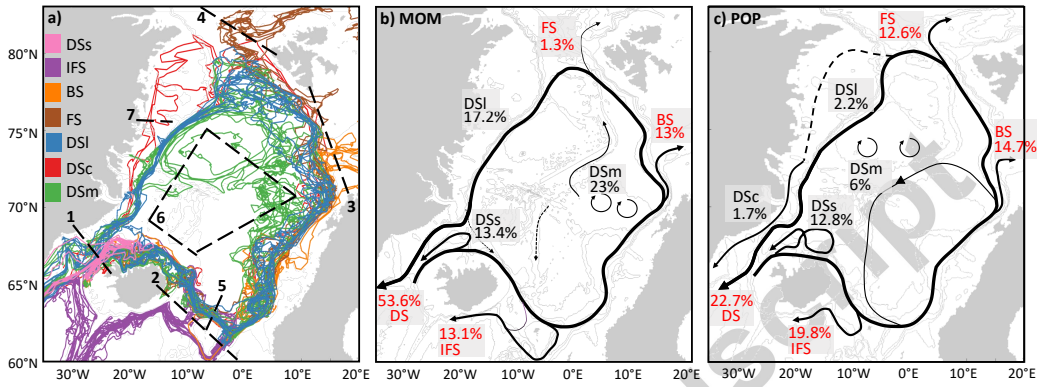

Fig. 6: (a) Example of 63 randomly chosen particle trajectories from both MOM and POP and their categorization (color coding). DSs (Denmark Strait short, pink) are particles that leave the Nordic Seas crossing transect 1, without crossing transect 5. IFS particles (Iceland-Faroe-Shetland, purple) are particles that leave by crossing transect 2. BS (Barents Sea, orange) are particles that travel into the Barents Sea crossing transect 3. FS (Fram Strait, brown) are particles that travel into the Arctic Ocean by crossing transect 4. DSl (Denmark Strait long, blue) are particles that travel along the rim of the Nordic Seas, crossing transects 5 and 1. DSc (Denmark Strait coast, red) are particles that follow the same route as DSl, but travel on the shelf region of Greenland crossing transect 7. DSm (Denmark Strait middle, green) are particles that enter the interior of the Nordic Seas indicated by box 6 and leave the Nordic Seas through transect 1. (b-c) The black arrows indicate the paths of the NIIC water in the Nordic Seas where the percentage gives the distribution of the NIIC watermass over the different pathways. The total fraction of the NIIC watermass that leaves through each exit is given in red. 19% (30.2%) of the particles are still in the Nordic Seas after 6 years in MOM (POP).

show a seasonal dependence in the two model simulations, the pathways of the NIIC watermass are not sensitive to the time of release of the particles.

Both models show the existence of a short loop along the inflowing NIIC back to Denmark Strait (the DSs path). At first sight, this path seems similar to the hypothesized path of Våge et al. (2011). However, only 13% of the volume that entered the Nordic Seas in the NIIC is taking this path in both MOM and POP, in contrast to the fast one-to-one connection between the NIIC and the NIJ proposed by Pickart et al. (2017). Furthermore, investigation of the particles' depth is needed in order to see whether this outward branch is actually part of the NIJ. To this end, the vertical distribution of the in- and outflowing branches of the different pathways at the Kögur section are visualised in Figures 7a and 7b. To derive this figure, the particles crossing this transect are mapped on a 0.1°x 10m longitude-depth grid. Only the contour that encompasses more than 80% of the particles is shown to highlight the main position of each pathway in the watercolumn.

In both models, most of the DSs watermass originates from the upper 100m of the NIIC (solid pink contour in Figures 7a-b), and this path is therefore shallower than the other paths. The particles follow the shelf break of Iceland and turn northwards at Kolbeinsey Ridge. In MOM, the particles return to Denmark Strait following the 1000m isobath along the Icelandic slope. In POP, some particles circulate in the Bloseville Basin (Figure 1) as well. On their outward journey, there is no indication in MOM that the DSs particles are connected to the NIJ, since the returning particles are all located in the upper 100m of the water column (pink dashed line in Figure 7a). In POP, however, there is a clear signal of outward flowing particles

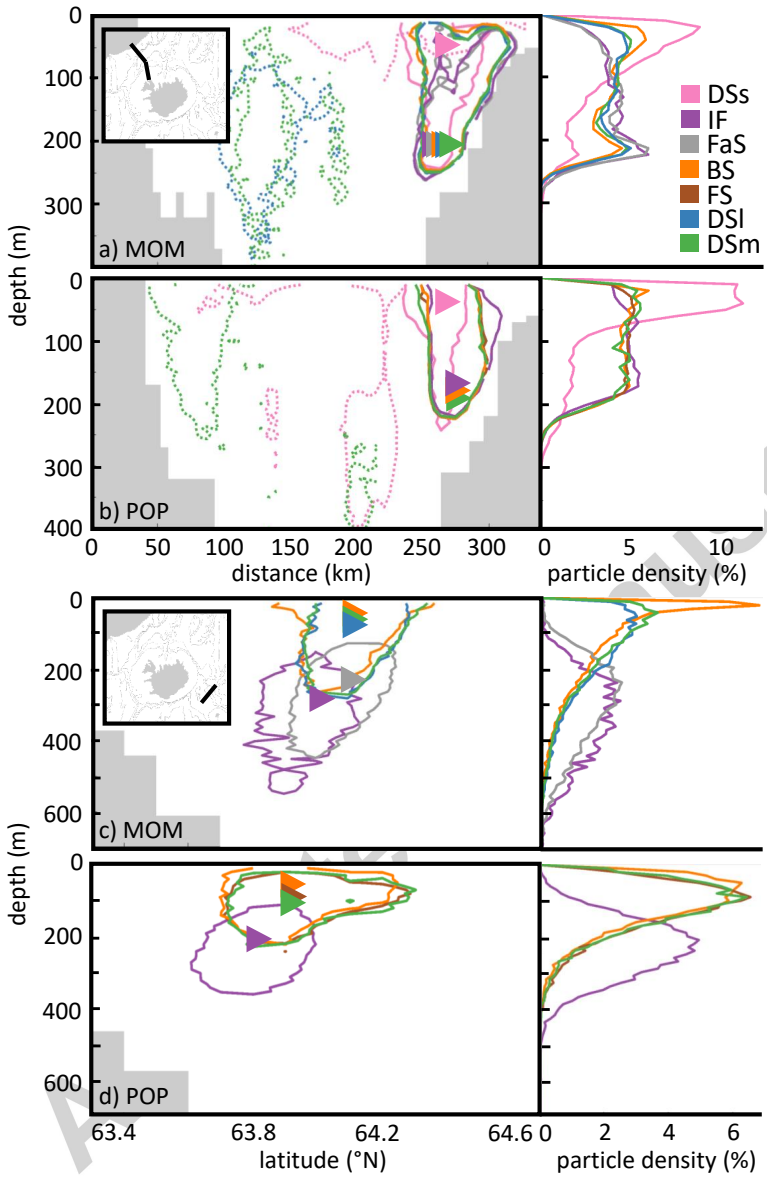

Fig. 7: The depth distribution of each pathway at (a,b) Kögur section and (c,d) a section east of Iceland (see inlays). The left panels show the contour, colored per pathway, that encompasses >80% of the particles. The triangles give the location where the maximum particle concentration of the pathway is found at these transects. The solid contours show the distribution of the particles that flow into the Nordic Seas, the dashed lines show the distribution of the pathways on their outward journey. The right panels show the normalized depth distribution of each path integrated along the transects. The IFS particles are separated in those that leave the Nordic Seas between Iceland and the Faroe islands (IF, in purple) and those that leave the Nordic Seas between the Faroe Islands and Scotland (FaS, in gray). Only the paths that carry more than 5% of the NIIC water are shown.

between 200m and 400m depth close to the Icelandic slope (pink dashed line Figure 7b), showing that in this model the outward branch is part of the NIJ. This indicates that the watermass transformation of the particles following the DSs path is different in both models. This will be further discussed in section 5.

As only 13% of the NIIC watermass takes the DSs path, the majority of the water is transported by other paths. A significant fraction of the NIIC watermass leaves the Nordic Seas between Iceland and the Shetland islands in both models (the IFS path, 13% in MOM and 20% in POP). In POP, all of the IFS particles leave the Nordic Seas between Iceland and the Faroe Islands (the IF path), whereas in MOM the majority of the IFS particles (>60%) leaves through the deeper channel between the Faroe Islands and Scotland (the FaS path). Again, the vertical distribution of the pathways is investigated by mapping the particles on a 0.1°x 10m latitude-depth grid of a transect east of Iceland (Figure 7c and 7d). Clearly, the IFS particles (purple color in Figure 7c-d) are located deeper in the water column than the particles of the other pathways. In MOM, the particles leaving between the Faroe Islands and Scotland are located slightly farther offshore. Therefore, they follow the 1000m isobath to the Faroe-Shetland Channel. The possible connection of the IFS path to the Iceland Scotland Overflow Water (ISOW) will be discussed in section 5.

Investigation of the vertical distribution of the pathways at the Kögur section and the transect east of Iceland gives insight why some particles flow south (the IFS path) and why some flow northward east of Iceland (the BS, FS, DSm, DSl and DSc paths). At the start of their trajectory, the

maximum concentration of the particles that do not take the DSs path is found at 200m depth in both models (see triangles in Figures 7a and 7b). However, east of Iceland, the particles that continue their journey north are all shifted upwards in the water column, whereas most particles that flow south are found below 200m depth (compare the purple and gray contours to the other colors in Figure 7c and 7d). The upper part of the water column east of Iceland is characterized by the Atlantic Water flowing north in the NwAC. Particles that are located near the surface are therefore likely to mix with the inflowing Atlantic Water and flow north, whereas the deeper particles follow the topography to the south.

These results indicate that processes that take place between the two investigated transects are crucial for setting the ratio of the southward and northward flowing fraction of the NIIC. The instability of the NIIC in this region (see Figure 3c-d) could provide one possible mechanism for setting these pathways apart. The generation of eddies coincides with local up- and downward movement of isopycnals and this process could separate particles in depth (Ypma et al., 2016). Another possible mechanism is that the particles are set apart in depth by local mixing within the mixed layer, which influences their density. It is beyond the scope of this study to determine the dominant processes in this region that are important for the transformation of the NIIC watermass. However, it is likely that the ratio of the southward and northward flowing fraction of the NIIC is subject to interannual variability.

The particles that flow north in the NwAC can take different routes. They either flow into the Barents Sea, flow through Fram Strait or return south along Greenland to Denmark Strait. One of the main differences be-

tween MOM and POP is that more than half of the NIIC watermass leaves through Denmark Strait in MOM, where most particles take the long way around (along the DSl and DSm paths). In POP, only 23% leaves through Denmark Strait, which may be explained by the weak EGC in POP and the long residence time of the particles in the Greenland Basin. Using a longer advection time of the particles would possibly increase the fraction of the NIIC watermass leaving the Nordic Seas through Denmark Strait in POP.

In summary, according to the two model simulations investigated in this study the connection between the NIIC and the NIJ is either weak (in POP) or non-existent (in MOM). Furthermore, the model simulations suggest a possible connection between the NIIC and the ISOW.

5. Watermass transformation along the pathways

In order to investigate the watermass transformation along the pathways of the NIIC water in the Nordic Seas, the temperature and salinity are traced for each particle. As an example, Figure 8a shows the trajectory of one of the particles that takes the DSl route in POP. Along this path, a net cooling and freshening of 7°C and 0.13 psu is seen (Figure 8b), leading to an increase in density of 0.68 kg/m^3. The transformation predominantly takes place at times when the particle is located inside the mixed layer (shaded periods in Figures 8b and 8c). Note that the magnitude of the cooling that takes place is not necessarily related to the depth of the mixed layer, neither to the strength of the heat flux at the surface. As seen in Figure 8b between location 1 and 2, the particle changes its thermohaline properties to a warmer and saltier watermass, while traveling to a location with a deeper mixed layer

and a stronger atmospheric cooling. Most likely, the warming and increase in salinity is a result of mixing with Atlantic Waters that enter the Nordic Seas east of Iceland. Two periods of strong cooling along the path of the particle can be distinguished. The cooling that takes place north of Iceland (upstream of number 1 in Figure 8a) at the start of the trajectory coincides with a reduction in salinity. This could indicate another mixing process with cold and fresh waters from the north. The second cooling event takes place when the particle is south of Svalbard (between location 6 and 7 in Figure 8a). During this cooling event, the salinity change is rather small and the particle is close to the sea surface, indicating that the reduction in temperature is most likely due to atmospheric cooling.

Note that, not only this particle, but all particles change their density predominantly, when they are located within the mixed layer. This is because diapycnal mixing below the mixed layer is small (e.g. Ledwell et al., 1993). In the model simulations, diapycnal mixing originates from the vertical background diffusion and in case of steep fronts from horizontal biharmonic diffusion. In addition to diapycnal mixing, there can be isopycnal mixing (mixing of temperature and salinity without a change in density) either by the explicitly resolved eddies or by horizontal diffusion. However, the effect of isopycnal mixing on temperature and salinity is much smaller than the diapycnal and diabatic water mass transformation within the ocean mixed layers. This is evident in Figure 8b-c from the much smaller temperature and salinity changes when the particle is below the mixed layer.

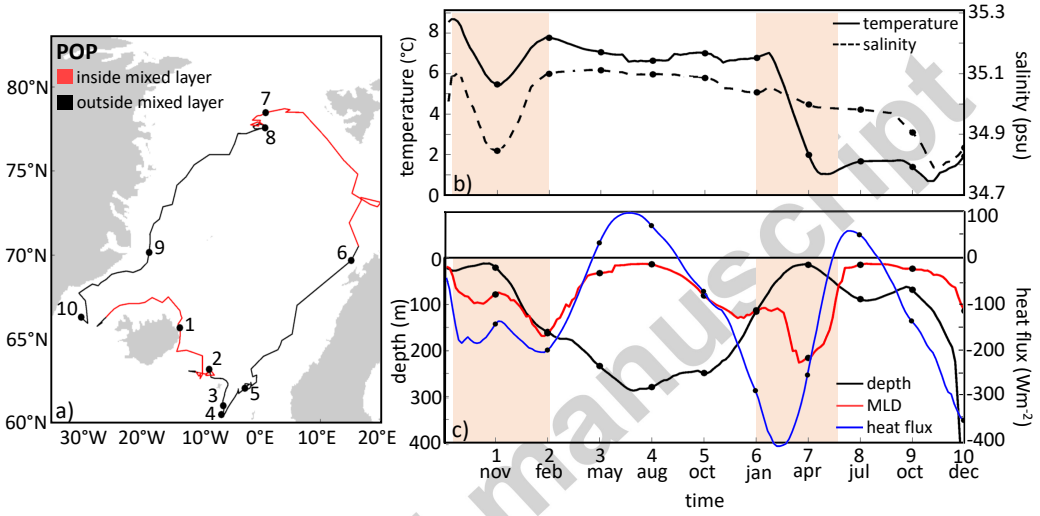

Fig. 8: (a) Example trajectory of a DSl particle in POP that is part of the DSOW. The line is red where the particle is traveling inside the mixed layer, the line is black outside the mixed layer. (b) Temperature (solid black line, left axis) and salinity (dashed black line, right axis) along the path of the particle trajectory shown in panel a. (c) Depth of the particle (in black), the mixed layer depth along the trajectory (in red) and the heat flux at the sea surface along the trajectory (in blue, negative means cooling). The shaded orange periods in (b-c) indicate when the particle is in the mixed layer. The numbers along the time axis of panel b and c correspond to the numbers in panel a, showing the particle location at the specified time.

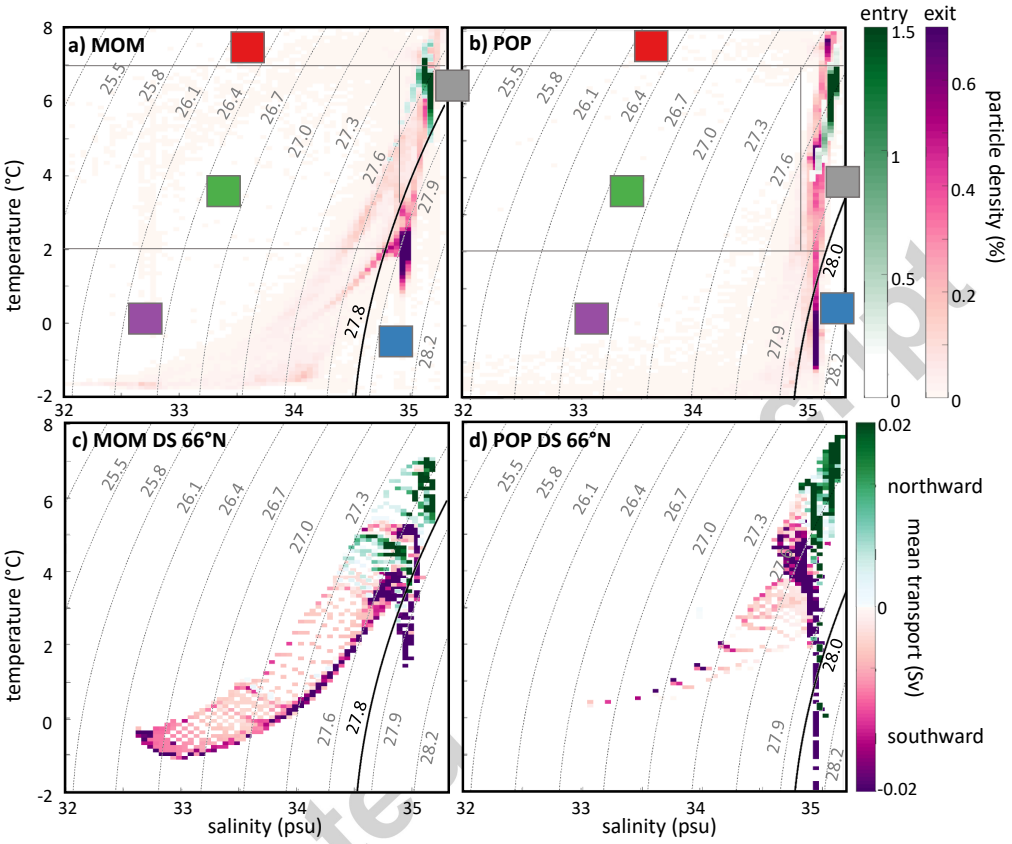

Fig. 9: (a-b) T-S diagrams of the thermohaline properties of the particles when entering the Nordic Seas (in green) and exiting the Nordic Seas at any of the exit locations (in purple) for (a) MOM and (b) POP. The transport weighted particle density is shown per $\Delta T = 0.1°\text{C}$ and $\Delta S = 0.05$ psu interval. The horizontal and vertical gray lines separate the T-S categories used in Figure 10. (c-d) Mean volume transport from the Eulerian velocity fields at Denmark Strait (66°N) as a function of temperature and salinity in MOM (left) and POP (right). Transport into the Nordic Seas is shown in green and transport out of the Nordic Seas in purple. In all panels, contours are density (kg/m^3), where the thick black line indicates the density threshold for the overflow waters (see section 3.3) in MOM respectively POP.

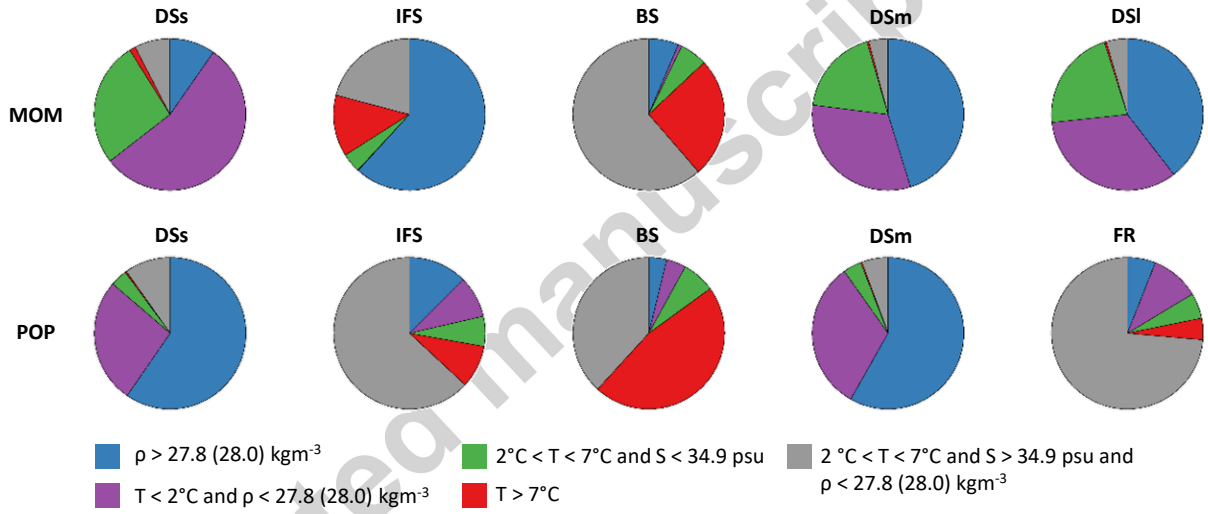

Fig. 10: Fraction of particles per pathway leaving the Nordic Seas within specific T-S categories, described in Figures 9a-b. Only the paths that carry more than 5% of the NIIC water are shown.

5.1. Contribution of the NIIC water to overflow waters

The investigation of this single particle pathway already elucidates many aspects of density changes that can occur in the Nordic Seas. To analyze the watermass transformation of the NIIC and its contribution to the overflows, all particles need to be taken into account. The change in temperature and salinity of the particles is visualized in the T-S diagrams in Figures 9a and 9b, where T-S properties of the particles that enter the Nordic Seas (in green) are compared to the T-S properties of the particles that exit the Nordic Seas at either Denmark Strait, crossing the Iceland-Scotland Ridge, into the Barents Sea or through Fram Strait (in purple). The temperature and salinity of the particles is gridded on a $\Delta T = 0.1°$C and $\Delta S = 0.05$ psu temperature-salinity grid. In both models a clear shift to lower temperatures is seen (ΔT $\sim$ 4-7°C) and little change in salinity.

Using the thermohaline properties of the particles, an estimate can be made to what extent the NIIC watermass contributes to the overflow waters in both models. Figures 9c and 9d show the mean volume transport of all the water crossing Denmark Strait as a function of temperature and salinity for MOM and POP, derived from the Eulerian mean velocity fields. The thick density contour shows the minimum density of the overflows defined in section 3.3. The same contour is also shown in Figures 9a and 9b. Using this threshold density, 27% (14.7%) of the water transported by the NIIC reaches a density that is larger than 27.8 kg/m^3 (28.0 kg/m^3) when leaving the Nordic Seas in MOM (POP).

To investigate along which paths this dense water is transported, the outflow temperature and salinity of the particles is split over five T-S cate-

gories, indicated by the gray lines in Figures 9a-b. The categories are based on whether the density along the pathway increased sufficiently to resemble the overflow (category 1), whether both temperature and salinity decreased (category 2), whether mainly the salinity decreased (category 3), whether the temperature increased (category 4), or whether the thermohaline properties of the particles remained roughly similar (category 5).

Applying this categorization process to each pathway (Figure 10) directly reveals along which pathways the dense water that eventually contributes to the overflows is transported (blue color in Figure 10). In MOM, the NIIC water that contributes to DSOW is transported mainly via the DSl and DSm path (18.2%, 0.20 Sv). In POP, 10.8% (0.19 Sv) of the NIIC water reaches Denmark Strait as DSOW, which is mainly transported via the DSs pathway and partly by the DSm path.

The NIIC watermass is also connected to the overflow between Iceland and Scotland (ISOW) in both models via the IFS path, and this connection is stronger in MOM than in POP (7.8%, 0.09Sv in MOM and 2.1%, 0.04Sv in POP). In MOM, the majority of the IFS particles are transformed to the overflow density (blue color Figure 10), whereas in POP most particles have T-S properties that are similar to those at entering the Nordic Seas (gray color Figure 10). However, just before entering the Iceland-Faroe Channel (at the transect shown in Figures 7c-d), the T-S properties of the particles in POP are very similar to those in MOM (not shown). A possible explanation for the sudden decrease in density is the slightly deeper mixed layer depths in the Iceland-Faroe Channel found in POP, making the IFS watermass more prone to mixing with the warm and salty Atlantic Water layer. This is linked

to the fact that the IFS particles in MOM leave mainly through the deep channel east of the Faroe Islands, whereas the IFS particles in POP leave west of the Faroe Islands (section 4). In both models the isopycnal that serves as the upper threshold for the overflow waters is located at ∼500m depth at the Iceland-Scotland Ridge. As the channel between Iceland and the Faroe Islands is only 500m deep, most of the ISOW has to leave east of the Faroe Islands, where the channel is 1100m deep.

Most of the particles that flow into the Barents Sea show either similar temperatures or an increase in temperature with respect to their original properties when flowing into the Nordic Seas. As a result, both simulations show only few particles with an overflow density entering the Barents Sea and the Arctic Ocean (1% in MOM and 1.8% in POP). It is likely that a part of the watermass that enters the Barents Sea and the Arctic Ocean will transform to denser waters further north, but this is outside the scope of this study.

5.2. Location of watermass transformations

To shed more light on the differences and similarities between the two model simulations regarding the watermass transformation along the paths, the location of the thermohaline changes along the pathways is investigated (Figure 11). The rate of change of temperature and salinity is determined and spatially binned on a 0.5°x 0.5° latitude-longitude grid. Next, this rate of change is multiplied by the residence time of the particles at each gridbox, to obtain the total change in temperature and salinity that the particles undergo at each location. Then, the results are averaged at every gridbox when the particle number in the gridbox exceeds 100 particles.

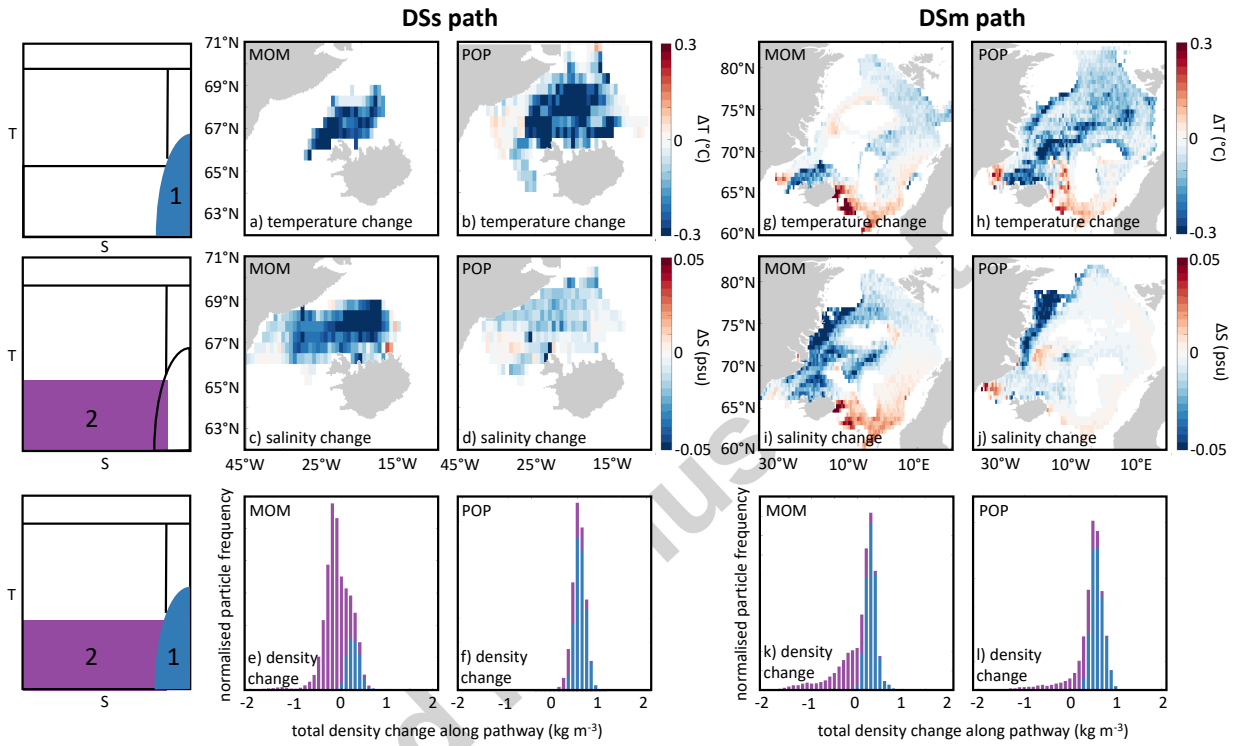

Fig. 11: Temperature change per 0.5x0.5° lon-lat gridbox (a-b, g-h), salinity change per 0.5x0.5° lon-lat gridbox (c-d, i-j) and total density change (e-f, k-l) along the DSs path (a-f) and the DSm path (g-l). The upper row shows the temperature change of the particles whose density at leaving the Nordic Seas is larger than 27.8 (28.0) kg/m^3 (T-S category 1, see Figures 9 and 10). The middle row shows the salinity change of the particles whose temperature and density properties at leaving the Nordic Seas are smaller than respectively 2°C and 27.8 (28.0) kg/m^3 (T-S category 2, see Figures 9 and 10). The third row shows the distribution of the total density change of each particle along the pathway (positive indicates a density increase), with the particles that connect to the DSOW (T-S category 1) in blue and the particles that leave the Nordic Seas with the T-S properties of T-S category 2 in purple.

The watermass transformation along the DSs path displays the largest difference between the two simulations. In MOM, the majority of the particles change their thermohaline properties to a fresher watermass (purple area Figure 10), whereas in POP a strong transformation to a cold and salty watermass takes place (blue area Figure 10). Figures 11a-b show the temperature change for the particles that leave the Nordic Seas as DSOW. Both simulations show strong cooling. In MOM, this cooling is confined to the region just north of Iceland, whereas in POP the water flowing along the DSs path cools over the entire area between Iceland and Greenland.

The differences between both model results become more apparent in Figures 11c-d, where the salinity change is shown for the particles that change their thermohaline properties to a colder and fresher watermass (T-S category 2, purple area Figure 10). Where in MOM the strongest cooling is found directly at the release location of the particles (66°N, Figure 11a), the strongest freshening takes place further downstream (∼68°N, Figure 11c). In POP, the reduction in salinity is significantly smaller and takes place closer to the Greenland coast (Figure 11d). The total density change along the DSs pathway (Figures 11e-f) indicates that the decrease in salinity in MOM outweighs the temperature decrease and most of the DSs particles become lighter along this path. In POP, the salinity decrease is small and most of the particles become denser along the DSs path (Figure 11f). This explains why the DSs particles are found at the surface in MOM and at depth in POP, when flowing south through Denmark Strait (Figures 7a-b).

The changes seen in the particles' properties along the DSs path can be related to the location of the sea ice (Figures 3a-b). As the maximum sea-

ice edge extends to the center of Denmark Strait in MOM, cooling by the atmosphere is confined to the region close to Iceland as seen in Figure 11a. In POP, the region between Iceland and Greenland is ice free year-round, and atmospheric cooling is not hindered by sea ice. Further, it is likely that mixing takes place with the cold and fresh waters that flow south along the Greenland coast. In MOM, the salinity gradient in the Denmark Strait region is much larger than in POP (see Figures 2e-f). The fresher surface waters seen in MOM can be due to the ice melt, but also due to the different surface freshwater boundary conditions. Therefore, similar mixing will lead to a stronger freshening in MOM than in POP.

The pathway along which the total density change is similar in both simulations is the DSm path (Figures 10 and 11k-l). However, the locations where the thermohaline changes take place are different. In MOM, the strongest cooling is found just north of Iceland, similar to the DSs path (Figure 11g), while in POP, cooling is also seen along the shelfbreak of Greenland and in the interior of the Nordic Seas (Figure 11h). Both models show freshening along the Greenland coast, where the water mixes with the Polar Water of the EGC (Figures 11i-j). In MOM, freshening is also seen just southeast of the Greenland Basin.

Both MOM and POP display local maxima of watermass transformation in the interior of the Nordic Seas (cooling in POP and freshening in MOM, Figures 11h-i). As seen in Figures 2h-i the flow speed is significantly lower in the interior of the Nordic Seas than at the boundaries and therefore the local maxima seen in Figures 11h-i are a result of the larger residence time of the particles in these areas. Just like for the DSs path, the atmospheric cooling

is limited by the sea-ice extent over the western side of the Nordic Seas in MOM as seen in Figure 11g and the freshening southwest of the Greenland Basin is likely a result of ice melt. The model simulations show an increase in both temperature and salinity southeast of Iceland. This transformation is a result of mixing with the Atlantic Water that flows into the Nordic Seas east of Iceland (Figure 1). The location of watermass transformation along the other pathways was investigated as well, but did not differ substantially from the watermass transformation along the DSm path shown in Figure 11g-j.

In summary, both simulations show a similar contribution of the NIIC to the DSOW of 0.2 Sv. However, the pathways along which the transformation takes place differ. This is a result of the differences in sea-ice cover in the Nordic Seas, and likely due to the different freshwater boundary conditions of the model simulations. As hypothesized in section 4, investigation of the thermohaline properties of the particles elucidated a weak connection between the NIIC and the ISOW.

6. Discussion and conclusions

In this paper Lagrangian particles have been used to investigate the pathways and the watermass transformation of the North Icelandic Irminger Current (NIIC) in the Nordic Seas in two ocean models. The volume of the NIIC water along each pathway and the contribution of the NIIC watermass to Denmark Strait Overflow Water (DSOW) and Iceland Scotland Overflow Water (ISOW) have been quantified. Further, the locations of the watermass transformation have been studied to investigate their relation to the location of the convection regions within the Nordic Seas.

Based on observations, some studies propose a strong connection between the NIIC and the DSOW, where the NIIC watermass is transformed northwest of the Iceland gyre and flows back into the Atlantic Ocean via the North Icelandic Jet (NIJ) through Denmark Strait (Våge et al., 2011; Pickart et al., 2017). The indication that both currents carry a similar volume transport and the assumption that the EIC does not contain a large part of the NIIC watermass, led to a suggested one-to-one connection between the NIIC and the NIJ (e.g. Pickart et al., 2017). The results from this study provide a different view than that deduced from the observations. The models suggest that the inflowing NIIC watermass is divided over several pathways in the Nordic Seas, and that only 13% of the NIIC watermass flows till Kolbeinsey Ridge to follow the short suggested loop. The region north of Iceland seems to play a crucial role in diversifying these pathways. The connection from the NIIC to DSOW via the NIJ has only been found in POP, since in MOM strong freshening takes place near the surface.

As was shown in Figure 7, the particles that follow the short DSs path originate from the upper 100m of the NIIC, whereas the deeper part of the NIIC flows farther east along Iceland. This could explain why Valdimarsson and Malmberg (1999) concluded that the DSs path was the main route for the NIIC, since this was the only path they could observe using surface drifters. Jónsson (1992) observed the NIIC watermass at the northeast corner of Iceland, slightly deeper in the watercolumn. In light of the results of our study, it is possible that he measured the fraction of the NIIC watermass that eventually leaves between Iceland and Scotland (the IFS path). Both models used in this study show a very strong watermass transformation

north of Iceland. Therefore it is possible that observations underestimate the Atlantic Water originating from the NIIC east of Iceland. Also, the part of the NIIC water that travels offshore of Iceland is indistinguishable from the EIC. Therefore, this study fits well with previous work that concluded that the EGC is most likely not the only source for the EIC (e.g. Logemann et al., 2013).

The results of this study strongly indicate that the DSs path is topographically controlled and that the fraction of the NIIC water following this path is set by the vertical structure of the current. Our results indicate that the path itself is not sensitive to sea-ice cover and atmospheric conditions and hence it is likely that similar conclusions can be drawn when repeating this research in models with interannually varying forcing. Further, as the instability of the NIIC is only slightly underestimated in the model simulations presented in this study, it is not expected that a fully eddy-resolving simulation would show a significantly stronger connection between the NIIC and the NIJ.

Both models display only 0.2 Sv NIIC contribution to the Denmark Strait Overflow Water, although the paths along which this water is transported back to Denmark Strait differ. This means that in these models the NIIC can not be the main source for the NIJ watermass. This is in line with the Lagrangian analysis conducted previously by Behrens et al. (2017), who found that only a small part of the DSOW originated from the NIIC. Note that as their study concerned only backtracking of the DSOW, no statement could be made on what fraction of the NIIC watermass contributes to the overflow as is done in this study.

Interestingly, both MOM and POP show a small contribution of the NIIC watermass to the ISOW of 7.8% respectively 2.1%, which is a weak connection that might be hard to detect by observations (e.g. Stefánnson, 1962; Perkins et al., 1998). Part of the Modified East Icelandic Water originates from the North Icelandic Shelf and is formed during winter convection and modified due to strong mixing with surrounding watermasses (Stefánnson, 1962; Read and Pollard, 1992). It is likely that the IFS path found in the models resembles this contribution.

The model simulations used in this study show agreement on both the pathways of the NIIC watermass and the contribution to the overflows, regardless of the large differences in the sea-ice cover, the hydrography and the circulation patterns between the simulations. This gives confidence that the conclusions drawn from the simulations regarding the NIIC pathways are not a model artifact, but apply to actual processes in the Nordic Seas.

The models do show some differences regarding the pathways along which DSOW is created. The agreement between the models in the NIIC contribution to DSOW of 0.2 Sv could therefore be a pure coincidence. In MOM, a mean freshening is seen along the DSs path and dense water is only transported to Denmark Strait along the deeper part of the EGC by the DSl and DSm paths. In POP, the EGC is weak and is only reached by a limited number of particles (2.2%). However, since the DSs path in POP does not display a strong decrease in salinity, this pathway serves as the main connection between the NIIC and the DSOW in this model.

The models have a very different approach regarding the sea ice, which might explain why the watermass transformation to DSOW is different. The

sea-ice cover in MOM between Greenland and Iceland is substantial and in POP non-existent (see black lines Figures 2b and 2c). Therefore, the strong freshening seen in MOM along the DSs path could be a result of sea-ice melt northwest of Iceland. Also the strength of the EGC seems to be affected by the location of the sea ice. It could be that a reduction in the sea ice in MOM would lead to a smaller decrease in salinity along the DSs path, leading to a larger contribution to DSOW. At the same time, the reduction in sea ice might lead to a stronger cooling of the EGC by the atmosphere which could resolve into a reduction of this current as is seen in POP. These relations are hypothetical and require further research outside the scope of this paper. What this study does show is that while the DSOW transport might be well captured by ocean models, the path of the dense water to Denmark Strait is highly sensitive to the hydrographic properties of the modeled ocean circulation.

In conclusion, this paper has shown that the connection between the North Icelandic Irminger Current and the Denmark Strait Overflow Water in MOM and POP is not as strong as proposed by observations. Furthermore, this paper confirms that the NIIC is connected to the Iceland Scotland Overflow Water as well. The watermass transformations taking place north of Iceland and the vertical structure of the NIIC play a crucial role in setting the future pathways of the NIIC watermass. The pathways along which the dense water is formed is different between the two models, highlighting the sensitivity to the model's representation of the hydrography and circulation in the Nordic Seas.

Acknowledgments

S.L. Ypma, S. Georgiou and N. Brüggemann were supported by NWO (Netherlands Organisation for Scientific Research) VIDI grant 864.13.011 awarded to C.A. Katsman. P. Spence was supported by an ARC DECRA Fellowship DE150100223. H.A. Dijkstra acknowledges support by the Netherlands Earth System Science Centre (NESSC), financially supported by the Ministry of Education, Culture and Science (OCW), Grant no. 024.002.001. Computing services for the MOM simulations were provided by the National Computational Infrastructure (NCI) in Canberra, Australia. Use of the SURFsara computing facilities for the POP simulations was sponsored by the Netherlands Organization for Scientific Research (NWO-E) under the project 15502. The model data used in the analyses in this paper has been described in Spence et al. (2017) (MOM) and Weijer et al. (2012) (POP). The observational dataset at the Kögur section was made available by Benjamin Harden. The altimeter products were produced by Ssalto/Duacs and distributed by Aviso+, with support from Cnes (https://www.aviso.altimetry.fr). We would like to thank five anonymous reviewers whose helpful comments greatly improved this paper.

Behrens, E., Våge, K., Harden, B., Biastoch, A., Böning, C.W., 2017. Composition and variability of the Denmark Strait Overflow Water in a high-resolution numerical model hindcast simulation. Journal of Geophysical Research: Oceans 122, 2830–2846.

Blindheim, J., Østerhus, S., 2005. The Nordic Seas, main oceanographic features. The Nordic seas: an integrated perspective , 11–37.

839 Courtois, P., Hu, X., Pennelly, C., Spence, P., Myers, P.G., 2017. Mixed layer
840 depth calculation in deep convection regions in ocean numerical models.
841 Ocean Modelling 120, 60–78.

842 Danabasoglu, G., Yeager, S.G., Bailey, D., Behrens, E., Bentsen, M., Bi, D.,
843 Biastoch, A., Böning, C., Bozec, A., Canuto, V.M., et al., 2014. North
844 Atlantic simulations in coordinated ocean-ice reference experiments phase
845 II (CORE-II). Part I: mean states. Ocean Modelling 73, 76–107.

846 Döös, K., 1995. Interocean exchange of water masses. Journal of Geophysical
847 Research: Oceans 100, 13499–13514.

848 Eldevik, T., Nilsen, J.E.Ø., Iovino, D., Olsson, K.A., Sandø, A.B., Drange,
849 H., 2009. Observed sources and variability of Nordic Seas overflow. Nature
850 Geoscience 2, 406.

851 Fer, I., Bosse, A., Ferron, B., Bouruet-Aubertot, P., 2018. The dissipation of
852 kinetic energy in the Lofoten Basin Eddy. Journal of Physical Oceanogra-
853 phy 48, 1299–1316.

854 Fetterer, F., Knowles, K., Meier, W., Savoie, M., Windnagel, A.K., 2017.
855 Sea Ice Index, Version 3 , Boulder, Colorado USA. NSIDC: National Snow
856 and Ice Data Center.

857 Griffies, S.M., Biastoch, A., Böning, C., Bryan, F., Danabasoglu, G., Chas-
858 signet, E.P., England, M.H., Gerdes, R., Haak, H., Hallberg, R.W., et al.,
859 2009. Coordinated ocean-ice reference experiments (COREs). Ocean Mod-
860 elling 26, 1–46.

Hansen, B., Østerhus, S., 2000. North Atlantic–Nordic Seas exchanges. Progress in Oceanography 45, 109–208.

Harden, B.E., Pickart, R.S., Valdimarsson, H., Våge, K., de Steur, L., Richards, C., Bahr, F., Torres, D., Børve, E., Jónsson, S., et al., 2016. Upstream sources of the Denmark Strait Overflow: Observations from a high-resolution mooring array. Deep Sea Research Part I: Oceanographic Research Papers 112, 94–112.

Harden, B.E., Renfrew, I.A., Petersen, G.N., 2015. Meteorological buoy observations from the central Iceland Sea. Journal of Geophysical Research: Atmospheres 120, 3199–3208.

Håvik, L., Pickart, R., Våge, K., Torres, D., Thurnherr, A., Beszczynska-Möller, A., Walczowski, W., von Appen, W.J., 2017. Evolution of the East Greenland Current from Fram Strait to Denmark Strait: Synoptic measurements from summer 2012. Journal of Geophysical Research: Oceans .

Jakobsen, P.K., Ribergaard, M.H., Quadfasel, D., Schmith, T., Hughes, C.W., 2003. Near-surface circulation in the northern North Atlantic as inferred from Lagrangian drifters: Variability from the mesoscale to interannual. Journal of Geophysical Research: Oceans 108.

Jochumsen, K., Moritz, M., Nunes, N., Quadfasel, D., Larsen, K.M., Hansen, B., Valdimarsson, H., Jonsson, S., 2017. Revised transport estimates of the Denmark Strait overflow. Journal of Geophysical Research: Oceans 122, 3434–3450.

de Jong, M.F., Søiland, H., Bower, A.S., Furey, H.H., 2018. The subsurface circulation of the Iceland Sea observed with RAFOS floats. Deep Sea Research Part I: Oceanographic Research Papers .

Jónsson, S., 1992. Sources of fresh water in the Iceland Sea and the mechanisms governing its interannual variability, in: ICES Marine Science Symposia, pp. 62–67.

Jónsson, S., Valdimarsson, H., 2005. The flow of Atlantic water to the North Icelandic Shelf and its relation to the drift of cod larvae. ICES Journal of Marine Science 62, 1350–1359.

Jónsson, S., Valdimarsson, H., 2012. Water mass transport variability to the North Icelandic shelf, 1994–2010. ICES journal of marine science 69, 809–815.

Köhl, A., 2010. Variable source regions of Denmark Strait and Faroe Bank Channel overflow waters. Tellus A 62, 551–568.

Korablev, A., Baranova, O.K., Smirnov, A.D., Seidov, D., Parsons, A.R., 2014. Climatological atlas of the Nordic Seas and northern North Atlantic .

Langehaug, H.R., Medhaug, I., Eldevik, T., Otterå, O.H., 2012. Arctic/Atlantic exchanges via the subpolar gyre. Journal of Climate 25, 2421–2439.

Large, W.G., McWilliams, J.C., Doney, S.C., 1994. Oceanic vertical mixing: A review and a model with a nonlocal boundary layer parameterization. Reviews of Geophysics 32, 363–403.

907 Large, W.G., Yeager, S., 2009. The global climatology of an interannually
908 varying air–sea flux data set. Climate Dynamics 33, 341–364.

909 Latarius, K., Quadfasel, D., 2016. Water mass transformation in the deep
910 basins of the Nordic Seas: Analyses of heat and freshwater budgets. Deep
911 Sea Research Part I: Oceanographic Research Papers 114, 23–42.

912 Ledwell, J.R., Watson, A.J., Law, C.S., 1993. Evidence for slow mixing across
913 the pycnocline from an open-ocean tracer-release experiment. Nature 364,
914 701.

915 Logemann, K., Ólafsson, J., Snorrason, Á., Valdimarsson, H., Marteinsdóttir,
916 G., 2013. The circulation of Icelandic waters - a modelling study. Ocean
917 Science Discussions 10.

918 Millero, F.J., Poisson, A., 1981. International one-atmosphere equation of
919 state of seawater. Deep Sea Research Part A. Oceanographic Research
920 Papers 28, 625–629.

921 Moore, G.W.K., Våge, K., Pickart, R.S., Renfrew, I.A., 2015. Decreasing
922 intensity of open-ocean convection in the Greenland and Iceland seas. Na-
923 ture Climate Change 5, 877.

924 Nilsen, J.E.Ø., Falck, E., 2006. Variations of mixed layer properties in the
925 Norwegian Sea for the period 1948–1999. Progress in Oceanography 70,
926 58–90.

927 Nurser, A., Bacon, S., 2014. The Rossby radius in the Arctic Ocean. Ocean
928 Science 10, 967–975.

929 Paris, C.B., Helgers, J., Van Sebille, E., Srinivasan, A., 2013. Connectivity
930 Modeling System: A probabilistic modeling tool for the multi-scale track-
931 ing of biotic and abiotic variability in the ocean. Environmental Modelling
932 & Software 42, 47–54.

933 Perkins, H., Hopkins, T., Malmberg, S.A., Poulain, P.M., Warn-Varnas, A.,
934 1998. Oceanographic conditions east of Iceland. Journal of Geophysical
935 Research: Oceans 103, 21531–21542.

936 Pickart, R.S., Spall, M.A., Torres, D.J., Våge, K., Valdimarsson, H., Nobre,
937 C., Moore, G., Jonsson, S., Mastropole, D., 2017. The North Icelandic Jet
938 and its relationship to the North Icelandic Irminger Current. Journal of
939 Marine Research 75, 605–639.

940 Read, J., Pollard, R., 1992. Water masses in the region of the Iceland–Faeroes
941 Front. Journal of Physical Oceanography 22, 1365–1378.

942 Richards, C.G., Straneo, F., 2015. Observations of water mass transformation
943 and eddies in the Lofoten Basin of the Nordic seas. Journal of Physical
944 Oceanography 45, 1735–1756.

945 Rudels, B., Quadfasel, D., Friedrich, H., Houssais, M.N., 1989. Greenland Sea
946 convection in the winter of 1987–1988. Journal of Geophysical Research:
947 Oceans 94, 3223–3227.

948 van Sebille, E., Spence, P., Mazloff, M.R., England, M.H., Rintoul, S.R.,
949 Saenko, O.A., 2013. Abyssal connections of Antarctic Bottom Water in a
950 Southern Ocean state estimate. Geophysical Research Letters 40, 2177–
951 2182.

Søiland, H., Chafik, L., Rossby, T., 2016. On the long-term stability of the Lofoten Basin Eddy. Journal of Geophysical Research: Oceans 121, 4438–4449.

Spall, M.A., 2004. Boundary currents and watermass transformation in marginal seas. Journal of Physical Oceanography 34, 1197–1213.

Spall, M.A., 2010. Non-local topographic influences on deep convection: An idealized model for the Nordic Seas. Ocean Modelling 32, 72–85.

Spence, P., Holmes, R.M., Hogg, A.M., Griffies, S.M., Stewart, K.D., England, M.H., 2017. Localized rapid warming of West Antarctic subsurface waters by remote winds. Nature Climate Change 7, 595.

Stefánnson, U., 1962. North Icelandic waters. Atvinnudeild Háskólans, Fiskideild.

Straneo, F., 2006. Heat and freshwater transport through the central Labrador Sea. Journal of Physical Oceanography 36, 606–628.

Swift, J.H., Aagaard, K., 1981. Seasonal transitions and water mass formation in the Iceland and Greenland seas. Deep Sea Research Part A. Oceanographic Research Papers 28, 1107–1129.

Tréguier, A.M., Theetten, S., Chassignet, E.P., Penduff, T., Smith, R., Talley, L., Beismann, J., Böning, C., 2005. The North Atlantic subpolar gyre in four high-resolution models. Journal of Physical Oceanography 35, 757–774.

Våge, K., Moore, G.W.K., Jónsson, S., Valdimarsson, H., 2015. Water mass transformation in the Iceland Sea. Deep Sea Research Part I: Oceanographic Research Papers 101, 98–109.

Våge, K., Papritz, L., Håvik, L., Spall, M.A., Moore, G., 2018. Ocean convection linked to the recent ice edge retreat along east Greenland. Nature Communications 9, 1287.

Våge, K., Pickart, R.S., Spall, M.A., Moore, G., Valdimarsson, H., Torres, D.J., Erofeeva, S.Y., Nilsen, J.E.Ø., 2013. Revised circulation scheme north of the Denmark Strait. Deep Sea Research Part I: Oceanographic Research Papers 79, 20–39.

Våge, K., Pickart, R.S., Spall, M.A., Valdimarsson, H., Jónsson, S., Torres, D.J., Østerhus, S., Eldevik, T., 2011. Significant role of the North Icelandic Jet in the formation of Denmark Strait overflow water. Nature Geoscience 4, 723.

Valdimarsson, H., Malmberg, S.A., 1999. Near-surface circulation in Icelandic waters derived from satellite tracked drifters. Rit Fiskideild 16, 23–40.

Weijer, W., Maltrud, M., Hecht, M., Dijkstra, H., Kliphuis, M., 2012. Response of the Atlantic Ocean circulation to Greenland Ice Sheet melting in a strongly-eddying ocean model. Geophysical Research Letters 39.

Wekerle, C., Wang, Q., Danilov, S., Schourup-Kristensen, V., von Appen, W.J., Jung, T., 2017. Atlantic Water in the Nordic Seas: Locally eddy-

permitting ocean simulation in a global setup. Journal of Geophysical Research: Oceans 122, 914–940.

Willebrand, J., Barnier, B., Böning, C., Dieterich, C., Killworth, P.D., Le Provost, C., Jia, Y., Molines, J.M., New, A.L., 2001. Circulation characteristics in three eddy-permitting models of the North Atlantic. Progress in Oceanography 48, 123–161.

Ypma, S., van Sebille, E., Kiss, A., Spence, P., 2016. The separation of the East Australian Current: A Lagrangian approach to potential vorticity and upstream control. Journal of Geophysical Research: Oceans 121, 758–774.